PERGAMON

Journal of Structural Geology 22 (2000) 1695–1711

JOURNAL OF STRUCTURAL GEOLOGY

www.elsevier.nl/locate/jstrugeo

Texture development of recrystallised quartz polycrystals unravelled by orientation and misorientation characteristics

Berndt Neumann[1]

Institut für Geologie und Dynamik der Lithosphäre (IGDL), Universität Göttingen, Goldschmidtstr. 3, D-37077 Göttingen, Germany

Received 2 December 1999; accepted 9 May 2000

Abstract

The development of microstructures and textures (i.e. crystallographic preferred orientations) during recrystallisation of naturally deformed quartz polycrystals has been studied via electron diffraction techniques in the scanning electron microscope. In the investigated sample series of quartz-rich rocks originating from different deformation regimes, the microstructural and textural changes in quartz have been significantly influenced by dynamic recrystallisation. Based on microstructural observations paired with orientation and misorientation analyses down to the scale of grains and subgrains, criteria could be established which characterise the dominant recrystallisation process and its influence on texture development. It is shown that the texture development during dynamic recrystallisation is controlled by a differential activation of slip systems in grains of 'soft' and 'hard' orientations. The analyses provide further evidence that specific grain orientations are preferred during crystal plastic deformation, recrystallisation and grain growth. The influence of twinning after the Dauphiné law was also investigated. Observations of a progressive reduction in the population of Dauphiné-twin boundaries during recrystallisation and a penetrative deformation in both hosts and twins indicate a generation prior to deformation and recrystallisation. A mechanical origin for twinning and possible influence on texture development was therefore discarded.

1. Introduction

Quartz texture analyses in naturally deformed quartzitic rocks have contributed importantly to the interpretation of deformation in these rocks. Together with experimental deformation studies (e.g. Green et al., 1970; Tullis et al., 1973) and numerical models (e.g. Etchecopar, 1977; Lister et al., 1978), the relationship between strain symmetry, finite strain axes and characteristic texture patterns can be established (see reviews by Schmid and Casey, 1986; Law 1990).

However, the relative importance of recrystallisation for texture development in contrast to the well-established concepts of deformation by intracrystalline slip (e.g. Hobbs 1985) has only been considered in relatively few studies (e.g. Urai et al., 1986; Jessell 1987, 1988a,b; Drury and Urai, 1990; Jessell and Lister, 1990; Wenk et al., 1997). This was mainly due to the difficulty in investigating mechanisms responsible for texture development with the traditional techniques, i.e. by utilising optical quartz-*c*-axis measurements or integrative X-ray measurements. With the advent of electron diffraction techniques in the scanning electron microscope (SEM), namely the orientation contrast (OC), electron channelling patterns (ECP) and electron back-scattered patterns (EBSP) techniques (see Dingley, 1984; Lloyd, 1987, 1994), it became feasible to measure complete crystallographic orientations of single crystallites with direct reference to the microstructure and therefore to address these shortcomings (e.g. Neumann, 1996; Lloyd et al., 1997; Trimby et al., 1998; Heidelbach et al., 2000). Examples of deformed rocks other than quartz are given by Leiss and Barber (1999), Prior (1999) and Fliervoet et al. (1999).

The aim of the present study was to investigate the microstructure and texture development, as well as the active mechanisms during recrystallisation of quartz-rich rocks from different deformation regimes. For that purpose two distinct sample suites were chosen, where plastic deformation and recrystallisation led to pronounced textures (i.e. crystallographic preferred orientations) and characteristic microstructures. Moreover, the samples were expected to show a clear textural and microstructural development since they represent two end-member cases of dynamic recrystallisation: grain growth due to dominant grain boundary migration (GBM) and grain refinement due to dominant subgrain rotation. It was attempted to find distinct

E-mail address: neumann-eos@t-online.de (B. Neumann).

[1] Present address: EO Elektronen-Optik-Service GmbH, Zum Lonnenhohl 46, D-44319 Dortmund, Germany.

0191-8141/00/$ - see front matter
PII: S0191-8141(00)00060-2

orientation and misorientation characteristics which will allow unambiguous distinction between the different recrystallisation processes. Another objective was to unravel the influence of crystal plastic deformation and recrystallisation on texture development on a grain and subgrain scale, as well as their relative influence on local orientations and misorientations.

These data are of vital importance for the quantitative modelling of texture development during recrystallisation (Jessell and Lister, 1990; Wenk and Christie, 1991) and may contribute to a better general understanding of texture development in quartz polycrystals.

2. Description of samples

2.1. Metaquartzites

The first sample suite consists of macroscopically homogeneous and coarse-grained metaquartzites. They stem from a several-hundred-metres-thick sequence of metaquartzites in the crystalline basement of the Heimefrontfjella mountain range (Antarctica), which were deformed under amphibolite grade conditions in the vicinity of the 'Heimefront Shear Zone'. The latter is a major dextral transpression zone, which was active during the Kibaran orogeny (Jacobs et al., 1993; Neumann, 1996). The transpressive character of deformation correlates well with observations of simultaneous folding and dextral shear deformation in the metaquartzite sequence. On the sample scale this is characterised by a pronounced rodding and a mineral stretching lineation parallel to the local fold axes. The foliation of the samples is weakly defined by the alignment of muscovite grains.

The investigated metaquartzite samples mainly consist of up to 97 vol.% quartz and a variable content (3–8 vol.%) of dispersed muscovite grains. The quartz microstructure is completely recrystallised and shows highly variable grain sizes of up to 5 mm and irregular grain shapes and boundaries due to an extensive grain growth by GBM. One of the metaquartzite samples can be separated into distinct domains with different average quartz grain sizes. The grain size differences in these domains are proportional to the variable muscovite content. These domainal grain size variations are here interpreted as a model for different stages in the recrystallisation or grain growth history. The two end members, a relatively fine-grained (1) and a very coarse-grained domain (2), were used for the detailed analyses presented below.

2.2. Quartz ribbon-bearing mylonites

The second sample suite consists of quartz ribbon-bearing mylonites, which were taken from a profile section across a small-scale sinistral shear zone in the Ivrea Zone, N Italy (for a further description see Dornbusch, 1995; Neumann, 1996). Similar high-temperature mylonitic shear zones of several decimetres- to hundreds-of-metres thickness are developed in all lithological units across the primary granulite facies of the NW part of the Ivrea Zone. Initiated during the Hercynian age, they formed a network of conjugated, shallow-dipping faults which were compensating for lateral extension of the lower crust (Rutter et al., 1993). After reactivation during a Triassic extensional phase they have been tilted into their present steep position during the alpine deformation (Schmid et al., 1987).

The investigated mylonite samples represent a profile from low- to high-shear strains, i.e. from margin to the centre of the shear zone. They show a characteristic *SC*-type fabric with an increasingly pronounced mylonitic foliation towards the shear zone centre. An incremental elongation and flattening of the quartz ribbons parallel to the mylonitic foliation is accompanied by a progressive grain refinement due to dynamic recrystallisation via subgrain rotation (see Section 4.2). The quartz ribbons are embedded in a matrix of recrystallised plagioclase, alkali feldspar and deformed orthopyroxene clasts. The microstructure and texture development of quartz occurred in an inhomogeneous manner due to strain-partitioning within different quartz ribbon domains and characteristic internal microfabric domains. The development is interpreted to be the result of a deformation increment at a late stage during shear zone development, subsequent to plagioclase recrystallisation. This late deformation mainly affected the quartz ribbons, which acted as the ductile phase within the 'hard' feldspar–pyroxene matrix. The two end members, i.e. the low- (1) and high-shear-strain sample (2) of the sequence, were chosen for the detailed analyses presented below.

3. Experimental techniques

3.1. Electron diffraction techniques

Backscattered electron (BSE) diffraction in the SEM has become an important tool for the combined study of microstructures and textures (i.e. crystallographic preferred orientations) in crystalline materials, which is often also referred to as microtexture analysis (Humphreys, 1988; Randle, 1992).

The following electron diffraction techniques in the SEM were used for the microtexture analyses presented below: OC imaging, ECP (here synonymously used with selected area channelling patterns) and EBSP. All these techniques result from the orientation-dependent scattering of incident electrons at the atomic lattice planes (Bragg-diffraction) within a (poly)crystalline material (for reviews see Lloyd, 1987, 1994; Dingley and Randle, 1992).

For the generation of OC, ECP or EBSP images the surface quality of the specimen is a critical factor. The procedures of specimen preparation, surface polishing and coating as well as their effects on image and pattern quality in geological specimens as applied in this study are

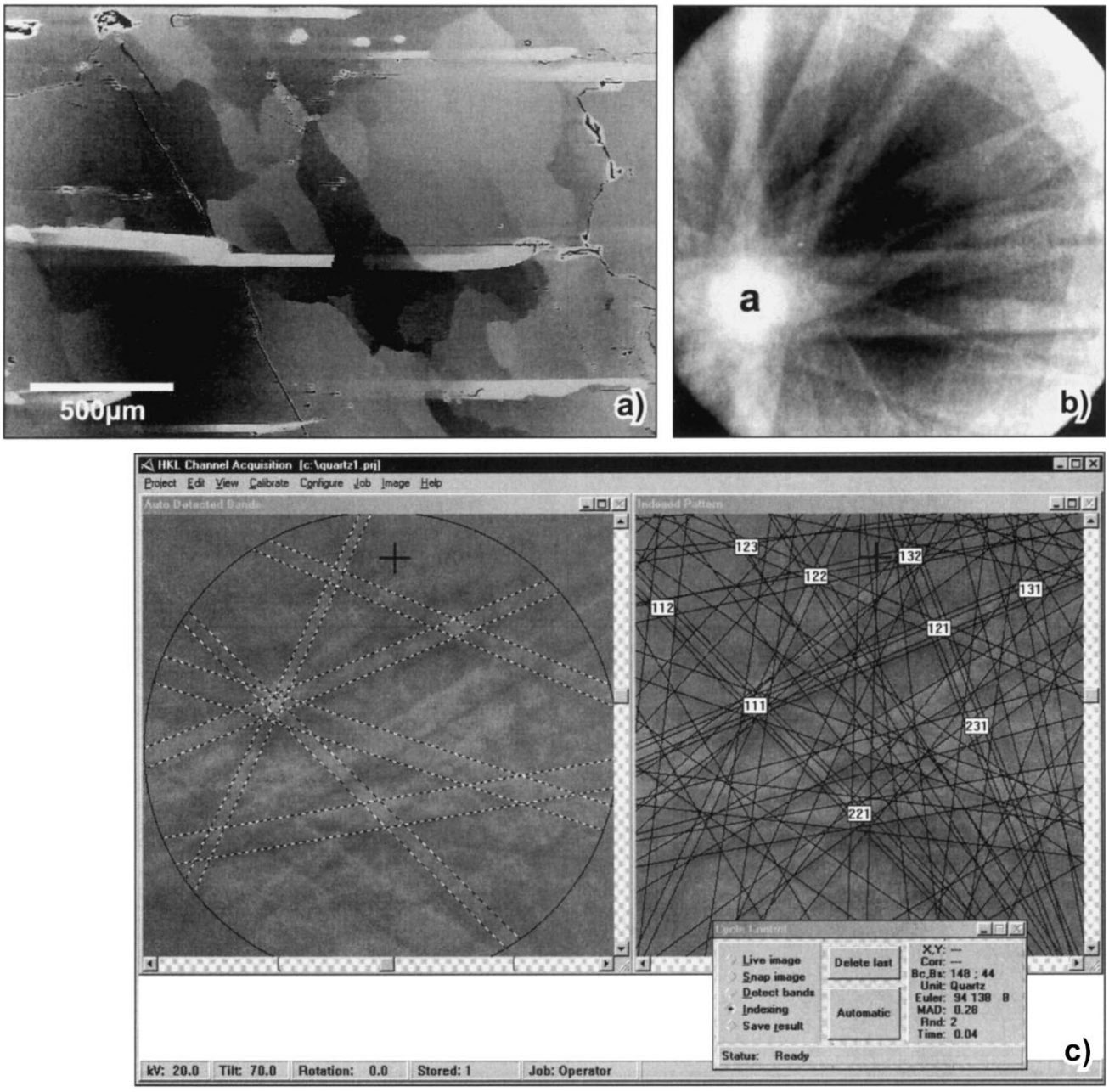

Fig. 1. Experimental: (a) OC image of quartz subgrain microstructure; (b) ECP of quartz close to *a*-axis; (c) crystallographic indexing of a quartz EBSP.

described in e.g. Lloyd (1987, 1994) and Neumann (1996). All samples were cut to square blocks with ~15 mm edge length and mounted in raisin cylinders. The blocks were then mechanically ground and polished in steps down to 0.25 μm diamond paste. To finally remove all surface damage the samples were chemically mechanically polished for 8–16 h using SYTON fluid. A thin carbon coat was applied to the samples in order to prevent charging.

The various techniques and detector strategies for generation of OC images with normal backscatter- or forward-scatter detectors (BSD) are referred to in Lloyd (1987) and Prior et al. (1996). In the present study a standard four-quadrant semiconductor BSD mounted to the pole piece of the SEM final lens was used for OC imaging (see e.g. Fig. 1a) as a basis for discrete orientation measurements with ECP and EBSP (see Fig. 1b and c).

The SEM used was a CamScan Series 4 instrument with additional dynamic focus in selected area diffraction mode, which allowed ECPs to be generated from areas down to ~3 μm. The acceleration voltage was usually 20 kV. By using a large aperture and spot size, high beam currents between 1 and 20 nA were applied to maximise the backscattered signal.

The techniques for crystallographic indexing and measuring

ECPs and EBSPs, as applied in this study, are reviewed by Lloyd (1987, 1994), Schmidt and Olesen (1989), Dingley and Randle (1992), and recently by Humphreys (1999).

3.2. Crystallographic considerations for quartz

As a consequence of Friedel's law, the backscattering intensity is identical for opposite directions in a crystal, so that the electron diffraction pattern always displays a centre of symmetry. Thus, the crystal symmetry is inherently reduced to Laue group symmetry.

In trigonal quartz (Laue group: $\bar{3}$m), the positive and negative rhombs r $\{10\bar{1}1\}$ and z $\{01\bar{1}1\}$ are discernible by the relative intensity of their diffraction bands. The $+a$ $\langle\bar{1}\bar{1}20\rangle$ and $-a$ $\langle11\bar{2}0\rangle$ directions can also be distinguished since their constituting diffraction bands appear as mirror images in the diffraction pattern. Therefore, an unambiguous crystallographic indexing of quartz to its true trigonal symmetry is possible. In addition, Dauphiné twins, which cannot readily be observed optically (require additional etching with HF), can be detected owing to their specific orientation relationship, characterised by a 180° or the equivalent 60° rotation around [0001]. However, owing to mirror planes occurring in diffraction patterns of quartz according to Friedel's law (cf. Olesen and Schmidt, 1990), a distinction between the left- and right-handed forms and therefore a detection of Brasil twins is not possible. All patterns are therefore indexed as right handed by convention.

3.3. Orientation and misorientation analysis

The microtexture measurements described in this study were obtained from single crystallite ECP and EBSP measurements using the CHANNEL software (Schmidt and Olesen, 1989; cf. Fig. 1c) as well as from fully automatic EBSP measurements using the orientation imaging microscopy (OIM) technique (Adams et al., 1993). Data presentation of the orientation and misorientation analyses was performed using programs developed by Farmer (1992) and Heidelbach (1994), as well as the CHANNEL + and the CHANNEL + ICE orientation mapping software from HKL Technology.

Both the ECP and EBSP techniques provided complete orientation data in the form of Euler angles, which were directly transformed into discrete pole figures of the main crystallographic directions c [0001] and a $\langle11\bar{2}0\rangle$ ($+a$ and $-a$ were not distinguished in the pole figures) and the poles to the main lattice planes m $\{10\bar{1}0\}$, r $\{10\bar{1}1\}$ and z $\{01\bar{1}1\}$. For some of the more detailed orientation analyses discussed below these directions and poles were displayed collectively in single pole figures. In order to locate specific maxima in the orientation and misorientation distributions, the orientation data were also used for calculations of the orientation distribution function and the misorientation distribution function (MODF) utilising programs developed at the Department of Geology and Geophysics, UC Berkeley (Wenk et al., 1998; Heidelbach et al., 2000).

The misorientations at the crystallite boundaries in quartz were described by rotation axis/angle pairs, calculated and displayed directly or via the MODF (Randle, 1992; Engler et al., 1994). By convention, the misorientation with the smallest rotation angle (ω_{min}) of all possible equivalents (six for trigonal crystal symmetry) was always chosen. The resultant maximum smallest rotation angle for trigonal quartz is 104.5°. For the analyses in this study only the misorientations between the neighbouring crystallites were calculated. They represent the 'correlated', i.e. the texture-dependent misorientation distribution (misorientations calculated between *all* single crystallites of a sample are referred to as the 'uncorrelated', i.e. the texture-independent misorientation distribution; see Pospiech et al., 1993). The misorientation data are displayed by histograms showing the frequency distribution of rotation angles ($\omega = 1$–104.5°), as well as by the distribution of rotation axes related to the sample coordinates (pole figures) and the crystal coordinates ('inverse' pole figures). In contrast to the 'uncorrelated' misorientation distribution of trigonal quartz, where the histograms usually show a continuous increase of rotation angles up to 80–90° which then decrease towards the maximum rotation angle of 104.5°, the 'correlated' misorientation distribution shows significant maxima and minima. These deviations from the 'uncorrelated' distribution can be interpreted as being related to the specific processes operative in the investigated samples (see below).

3.4. Interpretation in terms of slip systems

A concept of interpreting slip systems from misorientation axes at subgrain boundaries is presented in Fig. 2(a) and relates to the concepts of Lloyd and Freeman (1994), Lloyd et al. (1997) and Neumann (1996). It applies to slip due to edge dislocations resulting in a polygonized subgrain microstructure which dominantly consists of tilt boundaries (e.g. Nicolas and Poirier, 1976), as inferred from the straight and parallel boundary traces observed in the investigated samples. The orientation change during the activation of a single slip system can be described by a simple characteristic rotation in which the slip plane normal and slip direction change their orientation along a great circle with its pole being the rotation axis of the slip system. An example of a possible orientation change caused by basal $<$a$>$ slip during shear deformation is shown in Fig. 2(a). All other crystal directions rotate on small circles around this rotation axis and thereby result in the characteristic pole figure dispersion paths described by Lloyd and Freeman (1994). The rotation axis for each slip system has a constant crystallographic orientation which corresponds to the rotation axis of the misorientation between the crystallites involved. Fig. 2(a) and (b) shows the major slip systems in quartz with their associated rotation axes, as well as their representation in an 'inverse' misorientation pole figure. An inherent

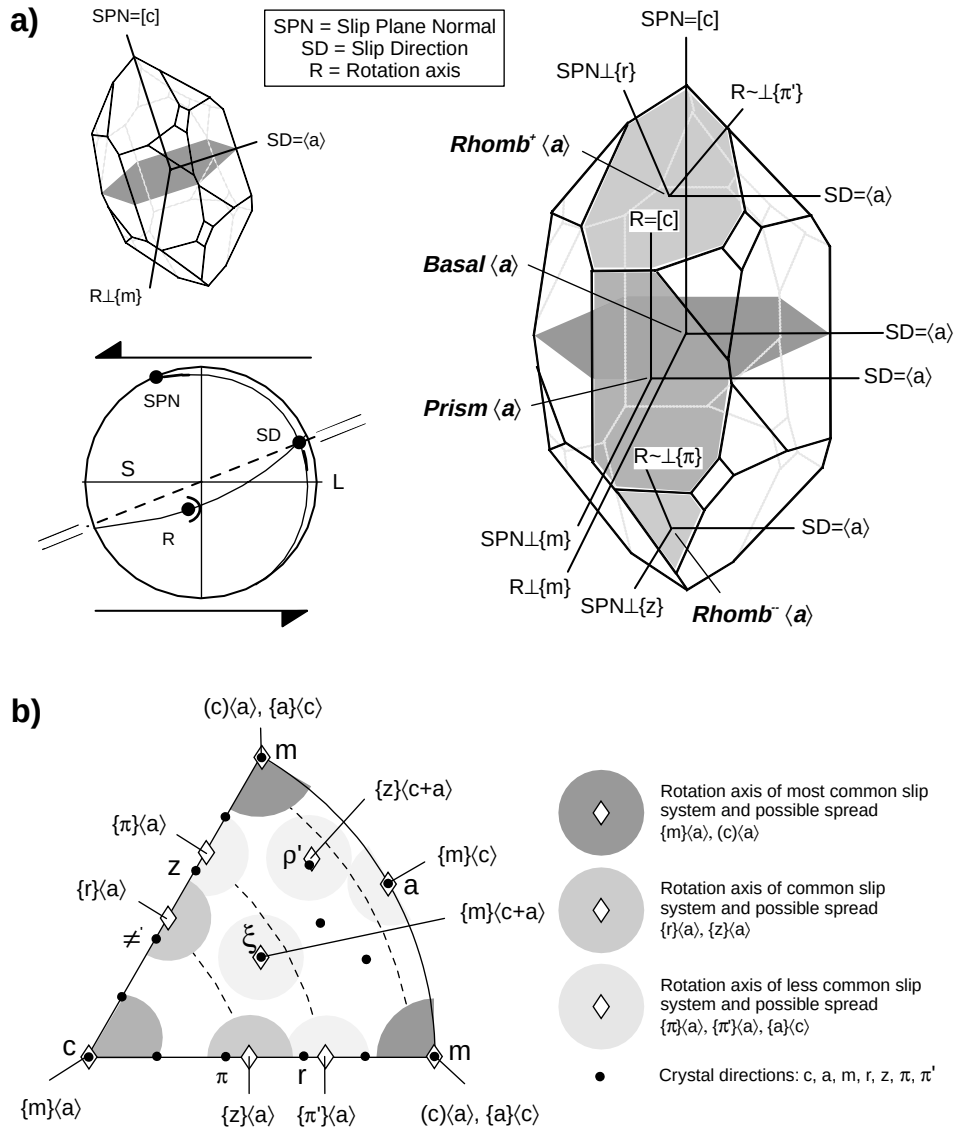

Fig. 2. Concept of interpreting slip systems from misorientation axes at subgrain boundaries generated by simple slip (valid for tilt boundaries): (a) possible orientation change due to basal <a> slip during simple shear deformation, and orientation of rotation axes of the most common slip systems of a quartz single crystal; (b) inverse pole figure with the orientation of crystal directions and rotation axes for common crystal slip systems in quartz.

problem with this approach is that the standard error in the orientation measurement has an increasing effect on misorientations with small rotation angles (<~10°) and causes the rotation axes for these misorientations to be less well defined (Prior, 1999). However, by the use of larger misorientation data sets this problem is reduced so that statistically significant clustering in the data can be interpreted in the way described above (cf. Fig. 8).

4. Results

4.1. Metaquartzites (quartz recrystallisation by dominant GBM)

Across the different grain size domains in the investigated sample a general texture strengthening with increasing average quartz grain sizes due to grain growth was observed. The grain-size variations in these domains are proportional to the variable muscovite content and result from GBM inhibition of quartz by the muscovite grains. They indicate different rates of recrystallisation but are interpreted here as a model for different stages in the quartz recrystallisation or grain-growth history which have been 'frozen in'. The 'development' of microstructures and textures is documented below by comparing the two end members within the sample, the fine-grained Domain 1 (with ~8 vol.% muscovite) and the coarse-grained Domain 2 (with ~3 vol.% muscovite).

4.1.1. Microstructures and textures

Fig. 3 gives an overview of the quartz microstructures

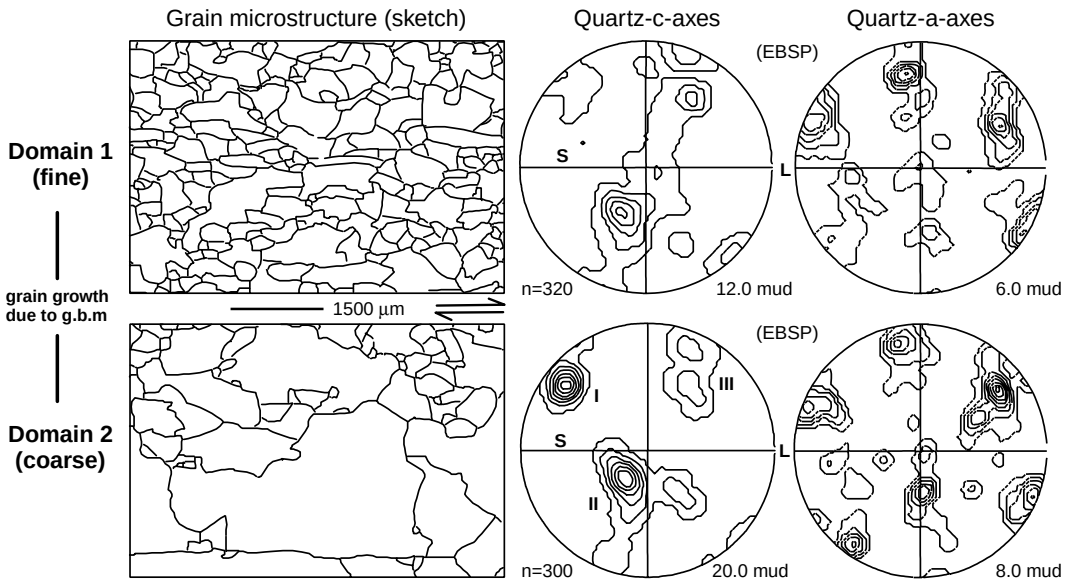

Fig. 3. Microstructural sketches, quartz-*c*- and *a*-axes pole figures derived from manual EBSP measurements in Domain 1 (fine grained) and Domain 2 (coarse grained) of recrystallised metaquartzites.

(sketch drawings) and textures derived from manual EBSP measurements (quartz-*c*- and -*a*-axis pole figures) encountered in the two investigated domains. An example of the quartz microstructure from a montage of OC images taken in the SEM is shown in Fig. 4. Both domains exhibit a completely recrystallised quartz microstructure with highly variable grain sizes from 50 μm up to 5 mm, documenting extensive grain growth. GBM is indicated by the irregular grain shapes and the abundance of concave/convex grain boundaries, as well as characteristic GBM microstructures (e.g. 'pinning', 'window' and 'left-over grains': see Jessell, 1987; Neumann, 1996). A coarse polygonal subgrain microstructure with variable subgrain sizes ranging from 50 μm up to 1 mm and straight subgrain boundaries is pervasively developed (cf. Figs. 4 and 10a). The muscovite grains are dispersed across the quartz microstructure and occur both along the quartz grain boundaries where they often show pinning of once-mobile quartz grain boundaries, as well as overgrown within the larger grains. From the microstructural observations above, a dynamic grain growth due to extensive GBM appears to be the dominant process for the microstructural development in quartz. Dynamic recrystallisation is interpreted as having occurred under high-temperature/low-stress conditions.

Domain 1 (fine) exhibits the lowest average and maximum grain size (230 μm and 1.6 mm circle-equivalent diameter, respectively) which relates to the weakest bulk texture observed within the sample (Fig. 3). The quartz *c*-axes are mainly distributed along a single oblique girdle with a dominant maximum closer to the centre (12 mud) and another maximum closer to the periphery of the pole figure. Together with another isolated maximum on the periphery of the pole figure, the distribution resembles a relic cross-girdle distribution. Although the textures show

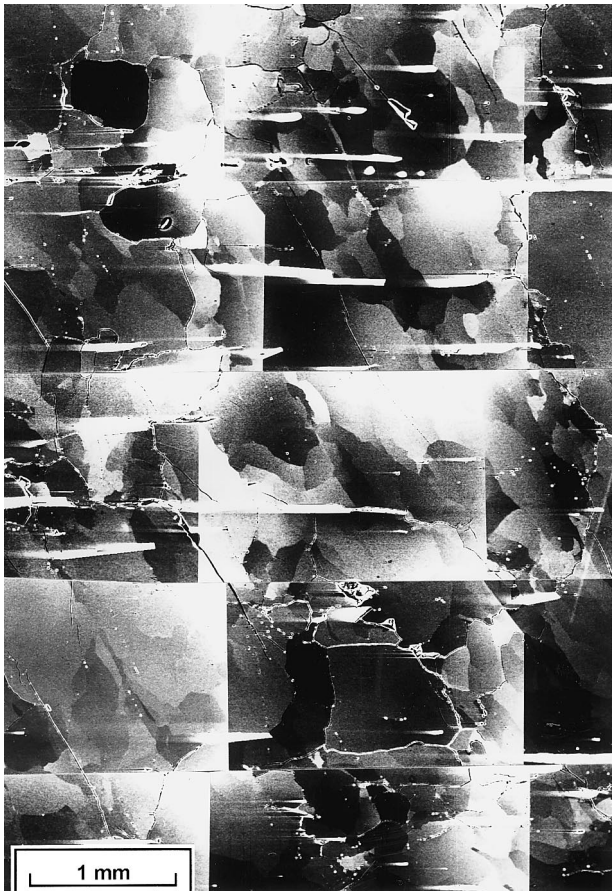

Fig. 4. Montage of OC images characteristic for a microstructure encountered in Domain 2.

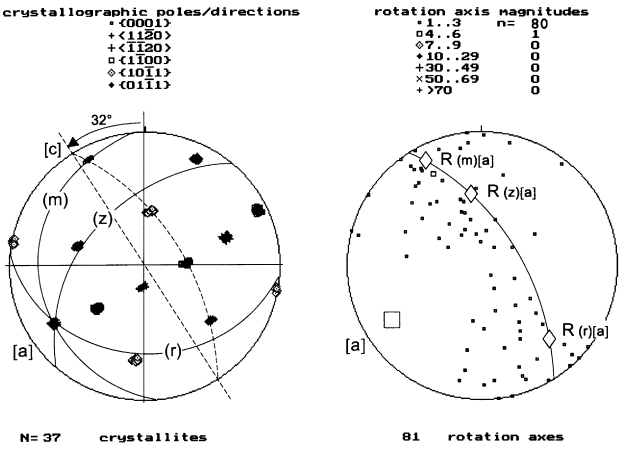

Fig. 5. Orientation and misorientation characteristics of neighbouring subgrains within a single grain domain showing a typical clustering of crystallographic poles/directions (*c*, *a*, *m*, *r*, *z*) and spread of subgrain misorientation axes (1–5°). The overlay indicates the orientation of possible slip systems and their respective rotation axes (domain orientation associated with Max. I, cf. Fig. 7a and b).

a triclinic symmetry and therefore indicate a complex deformation history, the quartz-*c*-axis texture pattern implies a dextral sense of shear during texture formation which was probably already established prior to the observed grain growth in the sample.

Domain 2 (coarse) shows the highest average and maximum grain size (450 μm and 3.0 mm circle-equivalent diameter, respectively) which relates to the strongest bulk texture of all investigated domains (Fig. 3). The quartz-*c*-axis texture is similar to the one in Domain 1, but with a prominent strengthening of the maxima at the expense of the overall girdle distribution. These dominant maxima are termed I, II and III according to their relative strengthening as compared with the *c*-axis texture in Domain 1. Max. I shows the most conspicuous increase in intensity and becomes the dominant maximum (20 mud). Max. II also shows an increase (but which is less pronounced than Max. I), whereas Max. III and the overall girdle distribution decrease in intensity.

In both domains, the quartz-*a*-axes describe in principle single crystal distributions around the dominant quartz-*c*-axis maxima, with an associated relative strengthening.

The different tendencies for growth and consumption can also be confirmed on the grain scale from axes distribution analyses [Achsenverteilungsanalysen (AVA), after Sander, 1950] of *c*-axes, as well as from the analysis of movement directions of grain boundaries between grains of the different texture maxima, deduced from characteristic GBM microstructures (cf. Neumann, 1996). Orientation maps generated from automated EBSP measurements are discussed below.

4.1.2. Misorientations

Fig. 5 shows a plot of crystal directions and misorientation axes of subgrains from within a single large grain of Domain 2 in exemplary fashion. The diagrams display a typical clustering of crystal directions, as well as a strong spread of misorientation axes with low rotation angles $<5°$. Even though rotation axes with small rotation angles $<10°$ are not well confined in orientation (see above), it appears that the axes in this example align in a non-random fashion. They can be attributed to a great circle which is perpendicular to one of the *a*-axes clusters in the pole figure (cf. Fig. 5).

Following the model for interpreting crystal slip systems described in Fig. 2, which appears to be applicable owing to the strong alignment of straight boundaries in the polygonised subgrain microstructure (cf. Figs. 4 and 10a), the slip systems which are most likely to be responsible for the distribution of rotation axes are indicated in Fig. 5. In this example of a single-grain domain with an orientation within Max. I, dominant prism- and rhomb-slip along the *a*-axis perpendicular to the rotation axis great circle can be deduced (similar to other grains of the same orientation). More conclusive data from statistically significant analyses applying automated EBSP measurements are presented below (cf. Figs. 7 and 8).

Fig. 6 shows the frequency distribution of misorientation angles resulting from the automated EBSP measurements presented in Fig. 7(a) and (b). The histograms of the two investigated domains are relatively similar, apart from a reduction in the total number of misorientations due to the general reduction of boundary area during grain growth.

The misorientation histograms show two distinct maxima. A first sharp peak occurs at very low rotation angles ($<5°$) and is related to misorientations at subgrain boundaries. Another sharp peak at 60° is associated with rotation axes in [0001] and represents Dauphiné twin boundaries, which are frequently observed in the orientations maps of Fig. 7(a) and (b). This peak is relatively reduced in Domain 2, which may indicate a consumption of twin boundaries during grain growth. All other rotation angles at high-angle grain boundaries show a relatively uniform frequency distribution ranging up to 95° and decreasing from there towards the maximum angle of 104.5°. In contrast to an 'uncorrelated' misorientation distribution, which predicts an overall decrease of high-angle boundaries with angles $> 60°$, the frequency of rotation angles between 65° and 95° here is even slightly enhanced. This can be explained by the high-angle misorientations of grain boundaries between the dominant texture maxima which are separated by appropriate angles, although they do not show significant maxima in misorientation space.

However, the most conspicuous feature in the histograms is the transition 'gap' at 5–15°, which covers the transition between low- and high-angle grain boundaries. It appears that the subgrain boundaries are not able to develop rotation angles $>5°$ before they are replaced by

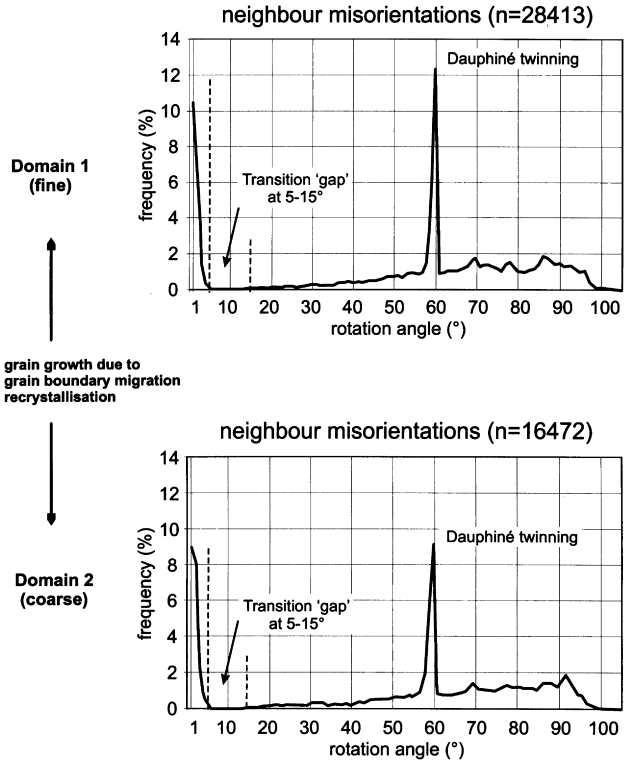

Fig. 6. Histograms showing the frequency distribution of misorientation angles calculated from the automated EBSP measurements in both domains of the metaquartzite sample (cf. Fig. 7a and b).

high-angle boundaries. The possible reasons for this will be discussed later.

4.1.3. 'Orientation maps' from automatic EBSP measurements

Orientation maps generated from automated EBSP measurements applying the OIM technique (Adams et al., 1993; Kunze et al., 1994) are shown in Fig. 7(a) and (b). The maps resemble the traditional approach for a AVA of quartz-*c*-axes, but are based on complete crystallographic orientations and misorientations calculated from the EBSP data.

The different shadings of grains within the orientation maps refer to Max. I, II and III of the quartz-*c*-axis texture. Together with the other crystal directions these maxima approximate single crystal orientations and can thus be described as discrete texture components in orientation space (Euler space). All orientation measurements which fall into these maxima with an orientation difference (i.e. misorientation angle) of less than 30° were shaded appropriately. The unshaded areas represent grains with an orientation difference of more than 30° to the dominant texture components, i.e. grains which represent the rest distribution.

Comparing Domain 1 with Domain 2, the orientation maps clearly show a growth of grain areas associated with Max. I and II, as well as a decrease of grain areas associated with Max. III and the relic *c*-axis girdle distribution. The area increase (>1) or decrease (<1) was determined by image analysis and quantified to a factor of 2.0 for Max. I, 1.4 for Max. II, 0.8 for Max. III and 0.5 for the rest distribution.

The pole figures displayed underneath the maps show similar tendencies in the strengthening of the appropriate *c*-axis maxima: factor 3.6 for Max. I, 2.3 for Max. II and 1.2 for Max. III. The pole figures derived from bulk neutron texture measurements performed on the same specimen document an excellent correlation with the automatically sampled discrete EBSP texture data (see pole figures at the bottom of Fig. 7a and b).

Also noticeable is the appearance of the Dauphiné twins interpenetrating the other grains with complex shapes. Their boundaries also appear to be mobile and often display similar characteristic GBM microstructures to the normal high-angle grain boundaries.

Fig. 8 shows misorientation distributions of subgrain boundaries (1–7.5°) in Domain 1 confined to the texture components of Max. I (representing the growing grains) and Max. III (representing the shrinking grains) calculated from the MODF (see above). Despite the small angular misorientations, the diagrams show statistically significant clusters, which can be interpreted in terms of active slip systems following the interpretation model in Fig. 2(b). The misorientation diagrams of Max. I show a generally stronger clustering and higher overall maxima than those related to Max. III. The maxima are well confined to only two dominant clusters close to the *c*- and *r*-poles which indicate strong slip in <a> on basal and rhomb planes (cf. Fig. 2b). In contrast, the misorientation diagrams related to Max. III show a more complex distribution with a lower overall maximum, indicative of a simultaneous activation of various interacting slip systems.

4.1.4. Pattern quality and subgrain microstructure

Apart from orientation data, the automatic EBSP analyses also provide a numerical figure for each orientation measurement, which specifies the pattern quality of each EBSP based on the contrast difference between a given number of bright diffraction bands and the overall contrast level (band contrast). The pattern quality figure, although normalised, is not completely orientation independent, but gives a qualitative measure of the lattice strains within the measured crystallites. Fig. 9 shows an example of such a pattern quality map. As in other pattern quality maps of the investigated samples an inverse correlation between internal strain and grain growth can be observed (cf. Neumann, 1996). The growing grains of Max. I and II display a generally higher EBSP quality than the shrinking grains associated with Max. III and the rest distribution. Furthermore, the growing grains have a lower internal contrast variation due to a lower density of dislocation clusters and subgrain boundaries.

The above observations on the pattern quality microstructure correlate well with observations on the optical

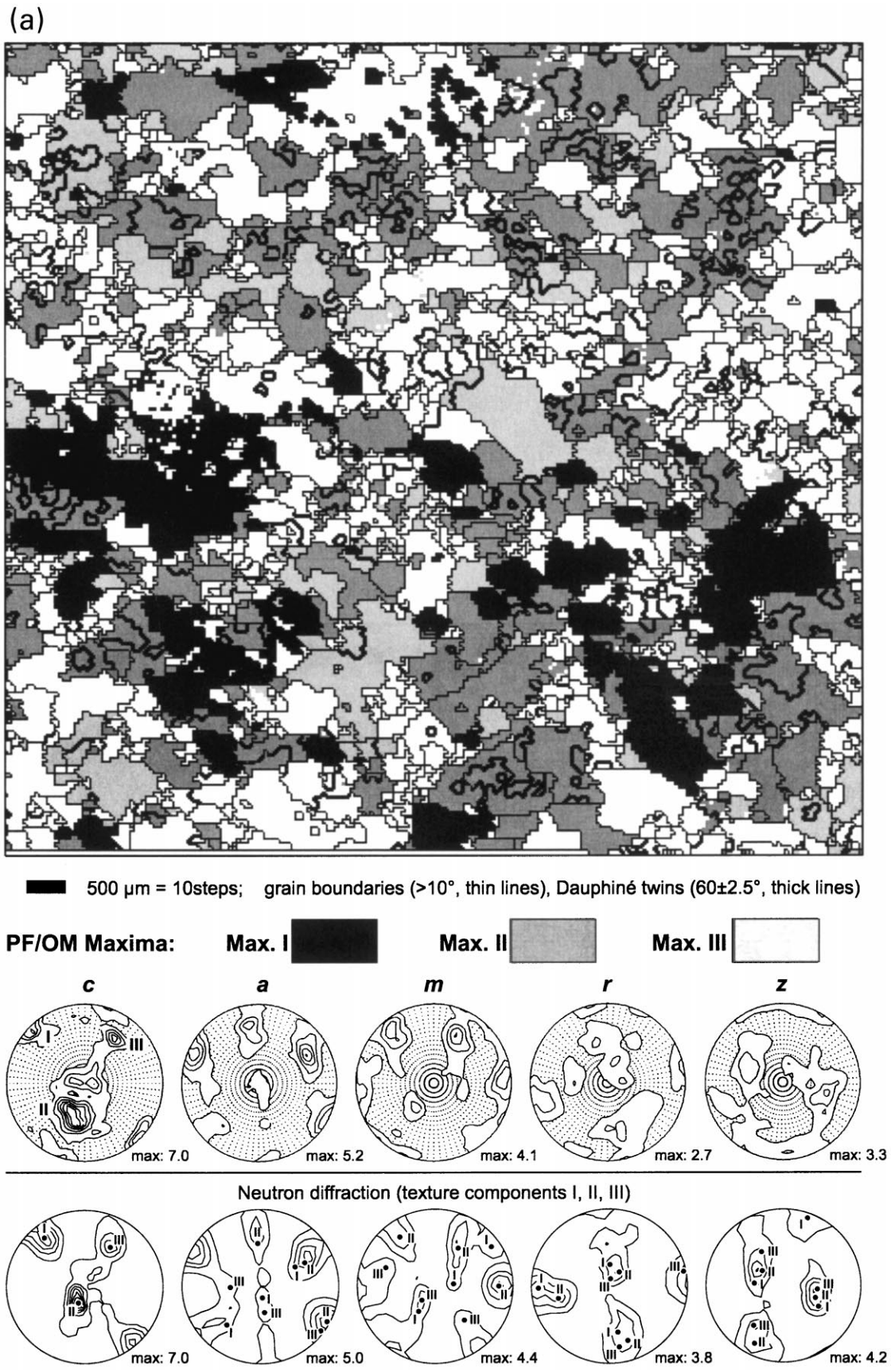

Fig. 7. Orientation maps generated by automated EBSP measurements. The different grey level shadings of grains within the orientation map refer to the dominant *c*-axis maxima or texture components I, II and III (maximum orientation difference of 30°). The boundaries levels refer to grain boundaries (>10°, thin lines) and Dauphiné twin boundaries (60° ± 2.5°, thick lines). The corresponding *c*-, *a*-, *m*-, *r*- and *z*-pole figures from EBSP and neutron texture measurements are compared at the bottom of the figures. (a) Domain 1 (fine grained) and (b) Domain 2 (coarse grained) of recrystallised metaquartzites.

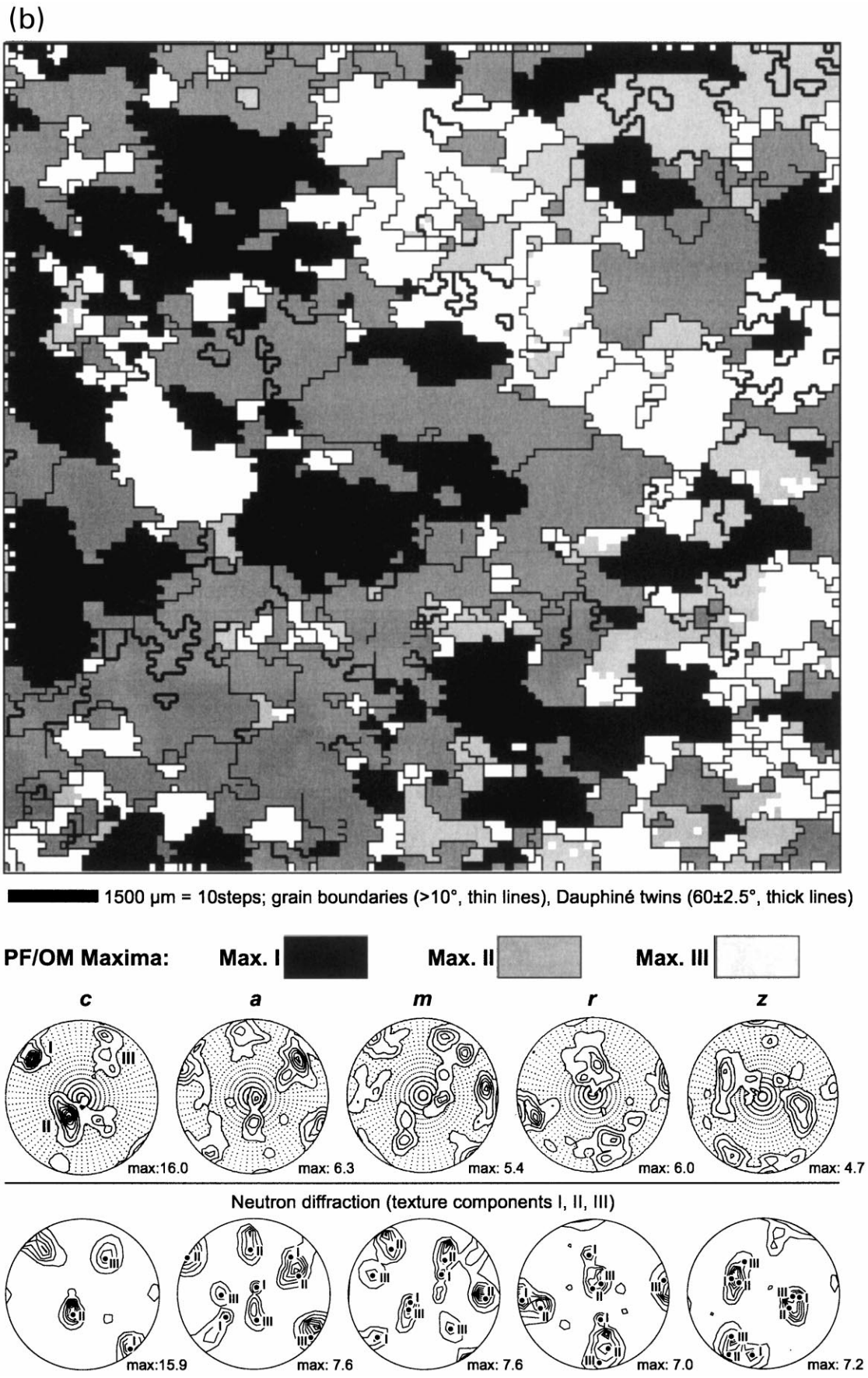

Fig. 7. (*continued*)

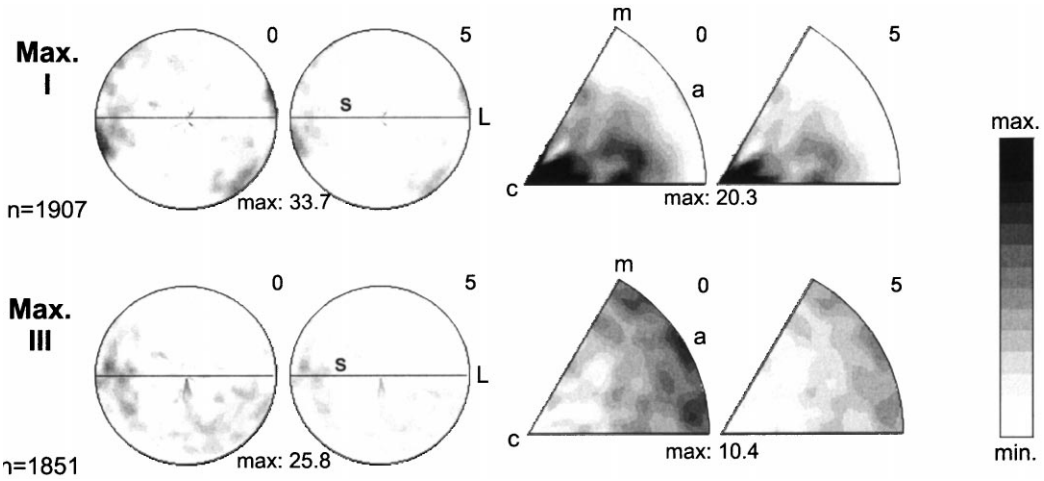

Fig. 8. Example of subgrain misorientation distributions from automated EBSP measurements (left: pole figures related to sample coordinates s and L; right: 'inverse' pole figures related to crystal coordinates). Comparison of MODF at low-angle misorientations ($\omega = 1–7.5°$) for Max. I (growing) and Max. II (shrinking) within Domain 1.

microstructure shown in Fig. 10. An AVA of quartz-*c*-axes, based on the tracing of grains and subgrains from an optical micrograph in Domain 2, shows grains from all *c*-axis Max I, II and III (Fig. 10a). The grains associated with Max. I and II are generally bigger and show a lower density of subgrains with parallel, widely spaced and straight boundaries. In contrast, the grains related to Max. III are smaller and display a higher density of closely spaced subgrain boundaries with a more irregular distribution. The strong alignment of subgrain boundaries within grains of Max. I results in a strong peak in the rose diagrams obtained from image analysis (see Fig. 10b), being inclined to the left at 35°. The subgrain boundaries of Max. II and III only form a small peak at ~40° to the right.

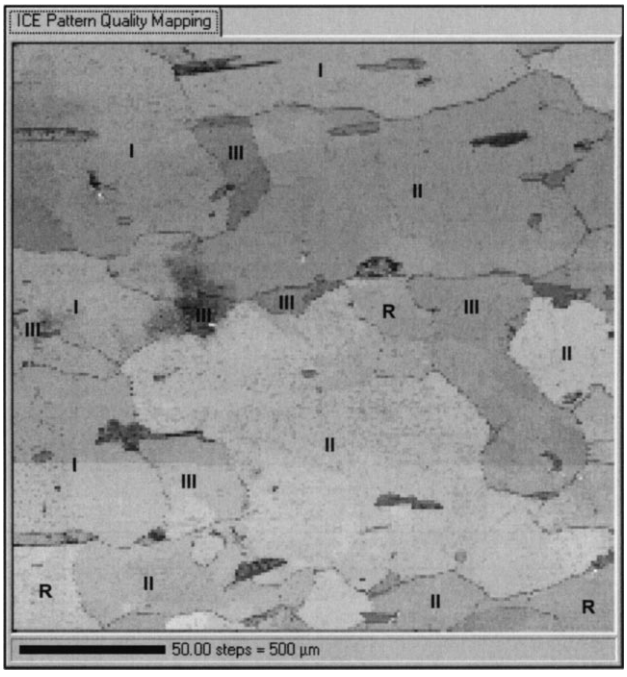

Fig. 9. Microstructural map obtained by automated EBSP measurements, based on the recorded pattern quality of each diffraction pattern (EBSP band contrast); shading ranges from good quality (bright grey levels) to poor quality (dark grey levels) patterns. The overlay labels I, II, III and R refer to the different texture components and 'Rest' distribution. Note the overall darker grey levels of Max. III and R compared with Max. I and II. However, owing to a certain orientation dependence of pattern quality and differing orientations of up to 30° within each texture component, the relative pattern qualities between the texture components are not always unambiguous.

The observations above document that, besides the general texture strengthening with increasing average grain sizes, the grain growth is strongly selective. Grains of the texture components Max. I and II grow preferentially at the expense of the grains with orientations in Max. III and the girdle distribution. The mechanisms and driving forces responsible for this are discussed in Section 5.

4.2. Quartz ribbon-bearing mylonites (quartz recrystallisation by dominant subgrain rotation)

4.2.1. Microstructures and textures

Fig. 11 gives an overview of the quartz ribbon microstructures (sketch drawings) and textures derived from manual ECP measurements (quartz-*c*- and -*a*-axis pole figures) in the two investigated end-member samples from the low-strain margin and the high-strain centre of the shear zone. Fig. 12 shows two characteristic microstructural domains from these samples in a montage of OC images taken in the SEM. The quartz ribbons in the margin of the shear zone are up to 2 mm wide and 2 cm long, and show a coarsely recrystallised microstructure due to GBM (100–500 μm) which is inherited from an earlier high-temperature deformation. The thicker quartz ribbons already show especially the beginnings of dynamic recrystallisation and grain refinement along the ribbon margins and grain boundaries. Moreover, elongated small subgrains and dynamically

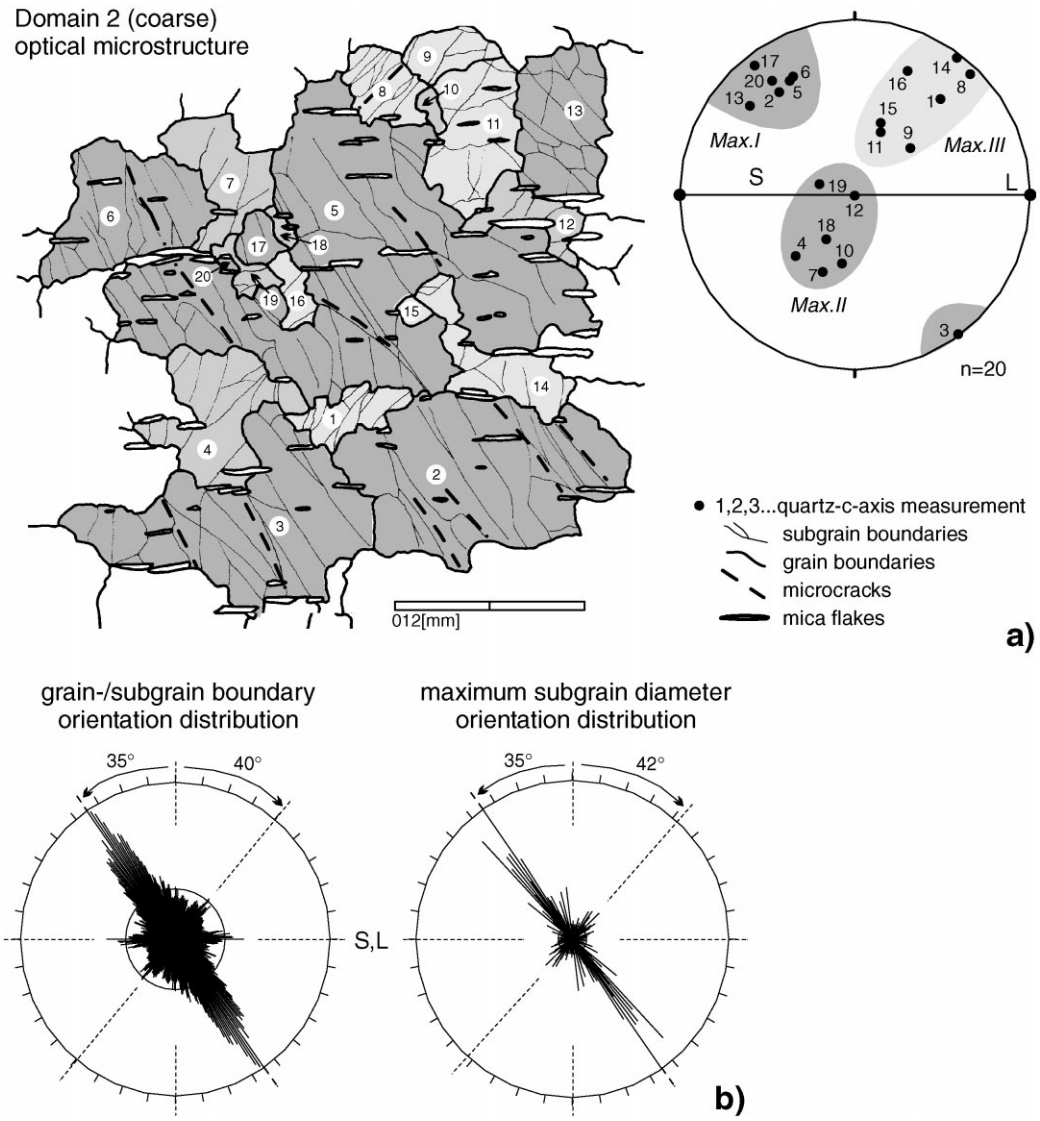

Fig. 10. Optical (subgrain) microstructure: (a) sketch map with boundaries and shading related to orientations in quartz-*c*-axis pole figure; (b) rose diagrams resulting from image analysis and showing the orientation distribution of boundary traces and maximum diameters.

recrystallised grains (5–50 μm) concentrate in characteristic internal domains of several-hundred-micrometres thickness, inclined at 35–45° to the mylonitic foliation, which occur in irregular intervals along the ribbons. The smaller quartz ribbons and isolated quartz in the feldspar matrix often consist of only a few or even single grains without significant substructures, indicating less strain build-up. With increasing shear deformation the quartz ribbons become further elongated and flattened, with subgrain formation and dynamic recrystallisation continuously developing along their entire length. At the centre of the shear zone the strongly deformed, thin (100–300 μm) quartz ribbons show a pervasive fine-grained (<5–50 μm) microstructure with a similarly oblique shape fabric at 35–45° to the mylonitic foliation.

The observed quartz microstructures in the ribbons indicate low-temperature and high-stress conditions during the late stage of deformation within the mylonites.

Sample 1 (low strain) shows the weakest bulk texture observed within the sample suite. The quartz *c*-axes (Fig. 11) represent an asymmetric cross-girdle distribution with a dominant maximum in the centre of the pole figure (10 mud). Together with an *a*-axis maximum close to the lineation and perpendicular to the sinistrally inclined *c*-axis girdle, the texture implies a sinistral sense of shear in correspondence to field and fabric observations. It has to be noted that the ECP measurements were mainly concentrated on the thicker quartz ribbons, which show stronger indications of internal deformation and beginning recrystallisation. Their texture is already dominated by the quartz-*c*-axis maximum in the centre of the pole figure. In contrast, the smaller quartz ribbons and matrix grains, which appear to be

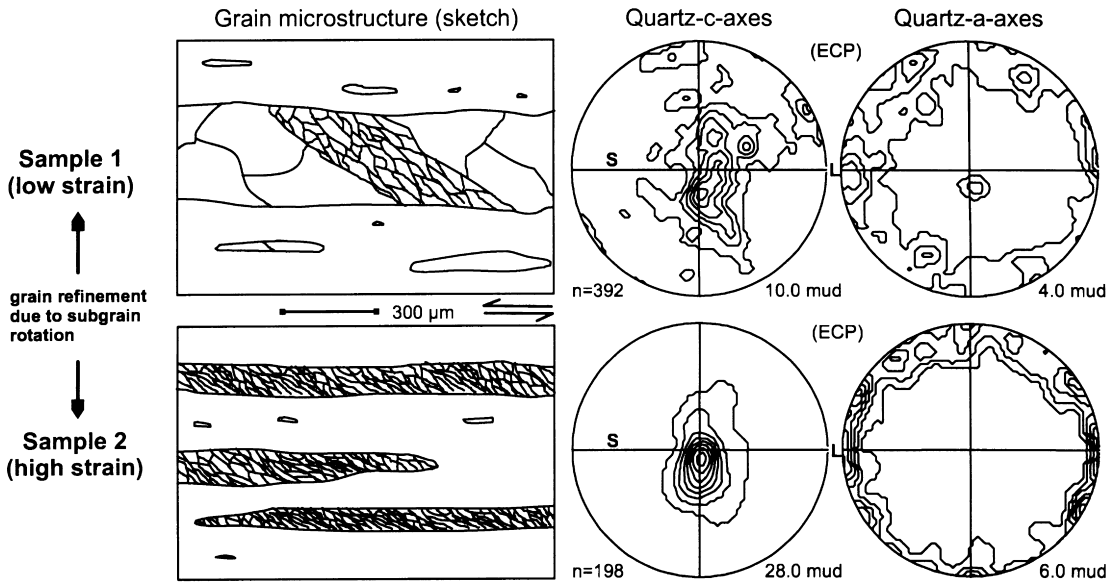

Fig. 11. Microstructural sketches, quartz-*c*- and *a*-axis pole figures derived from manual EBSP measurements in sample 1 (low strain) and sample 2 (high strain) of quartz-ribbon mylonites.

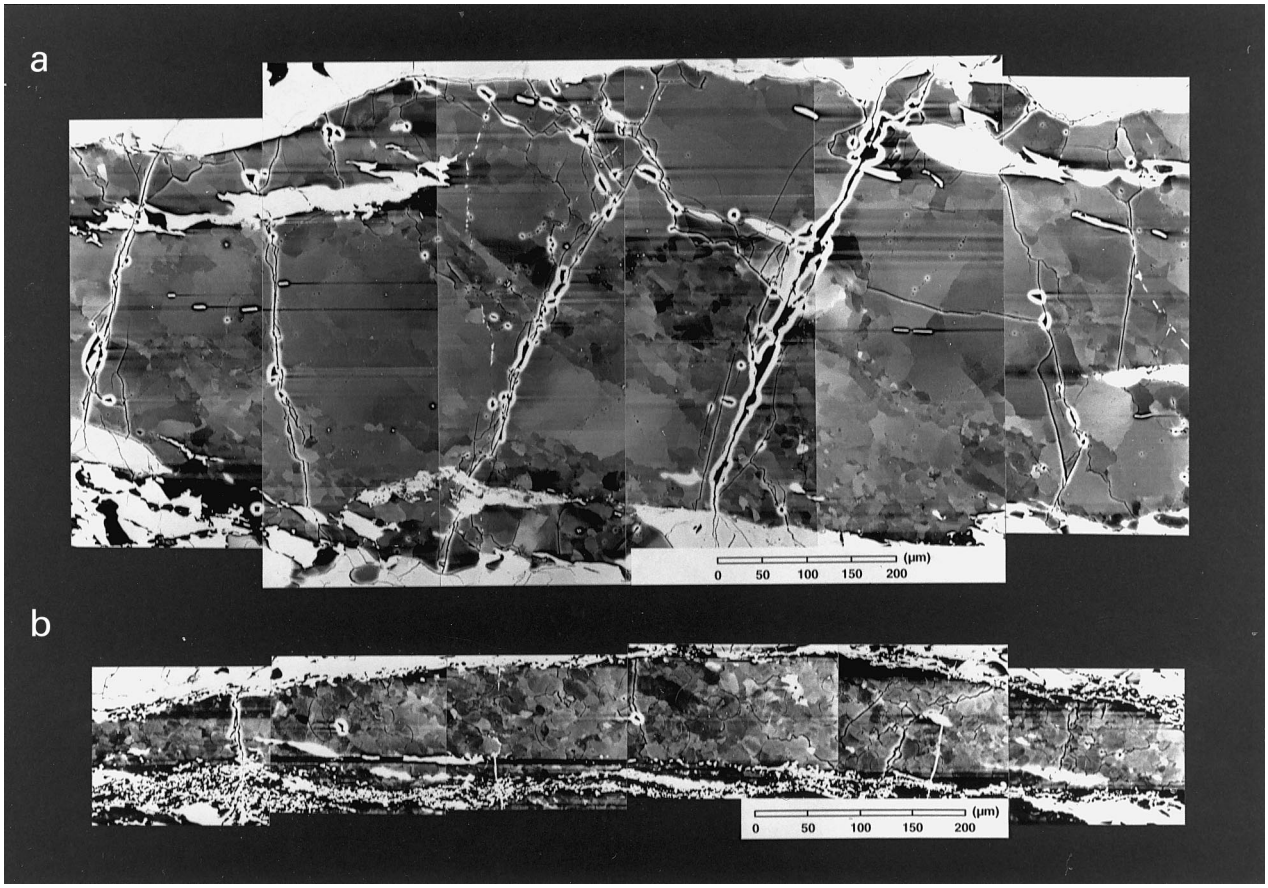

Fig. 12. Montage of OC images characteristic for a microstructure encountered in (a) sample 1 (low strain) and (b) sample 2 (high strain) of quartz-ribbon mylonites.

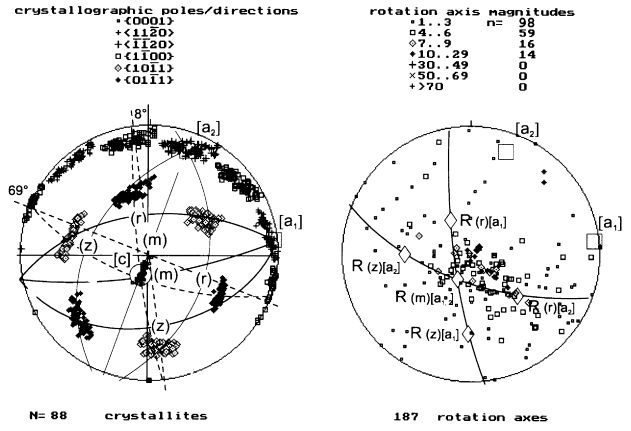

Fig. 13. Orientation and misorientation characteristics of neighbouring subgrains within a single grain ribbon domain showing a typical clustering of crystallographic poles/directions (*c*, *a*, *m*, *r*, *z*) and spread of subgrain misorientation axes (1–15°). The overlay indicates the orientation of possible slip systems and their respective rotation axes (domain orientation associated with dominant *c*-axis maximum in the centre of the pole figure).

relatively strain free, often represent the girdle texture components but are statistically underrepresented in the measurements. Therefore, the textures do not completely represent the overall bulk texture of the lower strain samples, as measured with other techniques (see Dornbusch, 1995; Neumann, 1996), and indicate a strongly domainal texture development and strain partitioning among the different ribbon domains.

Sample 2 (high strain) shows the strongest bulk texture of the sample suite. In contrast to sample 1, the quartz-*c*-axes are clustered in the dominant maximum in the centre of the pole figure (28 mud). The quartz-*a*-axis maximum is more pronounced and now aligned with the lineation (cf. Fig. 11). This texture and accompanied recrystallisation microstructure is pervasively developed across all quartz ribbon domains.

4.2.2. Misorientations

Fig. 13 shows an example of a plot of crystal directions and misorientation axes of subgrains from a characteristic oblique microfabric domain within a quartz ribbon. The diagrams display typical dispersions of the crystal directions, as well as a clustering of misorientation axes with low rotation angles (<15°) close to the centre of the pole figure.

Following the interpretation model of Fig. 2, which is similarly applicable owing to the strong shape fabric of the polygonised subgrain microstructure, the slip systems responsible for the distribution of rotation axes are indicated in Fig. 13. The example domain approximates a single grain with strong axial dispersion of its constituting subgrains with a *c*-axis orientation close to the centre of the pole figure. This orientation is present in both samples and therefore believed to be a stable orientation during dynamic recrystallisation. The clustering of rotation axes as well as the axial dispersion paths indicate dominant prism- and

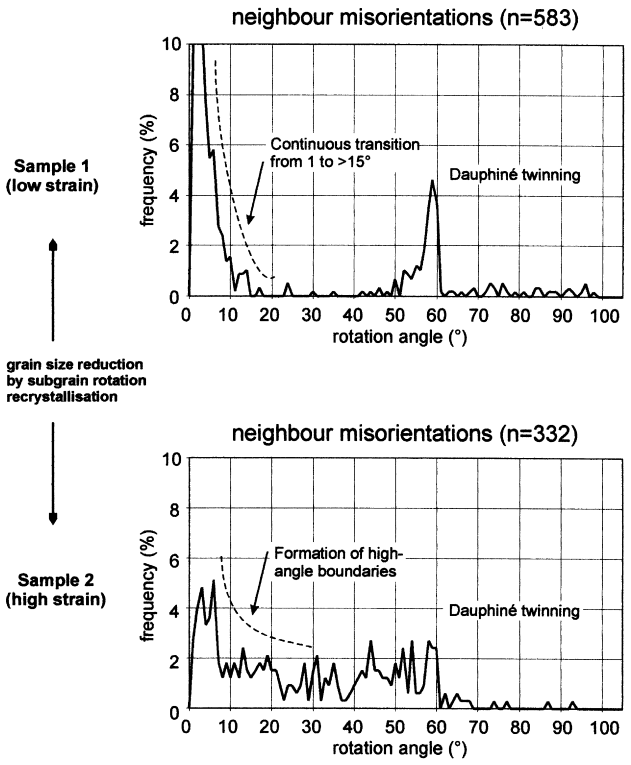

Fig. 14. Histograms showing the frequency distribution of misorientation angles calculated from the manual ECP measurements in both samples of the mylonite sequence.

rhomb-slip related to two different *a*-axes on the periphery of the pole figure.

Fig. 14 shows the frequency distribution of misorientation angles calculated from all neighbouring crystallites within each sample obtained via manual ECP measurements. The misorientation histograms from the two investigated samples show significant differences.

The histogram of sample 1 (low strain) shows a strong peak at low rotation angles (<15°) indicative of the misorientations at subgrain boundaries but which is broader than the peak observed in the diagrams of the metaquartzite samples (cf. Fig. 6). The smoother slope of the peak towards higher rotation angles indicates a continuous transition from low- to high-angle boundaries. The other conspicuous peak close to 60° is again associated with rotation axes in [0001] and represents Dauphiné twin boundaries. None of the other angles shows any significant accumulation.

In contrast, the histogram of sample 2 (high strain) shows a more randomised distribution of misorientations with a decrease of the low-angle and Dauphiné twin peaks, together with an increase of high-angle boundaries between 10 and 60°. This can be interpreted in terms of a progressive formation of high-angle boundaries due to the continuous rotation of subgrains. In both cases a low frequency of high-angle boundaries (>60°) is evident.

The observations above document that the texture development is strongly domainal. The development occurs due to strain partitioning within the different quartz

ribbon domains and characteristic internal microfabric domains. Also in this case the dynamic recrystallisation is strongly selective. Grains with an orientation close to the strong *c*-axis maximum in the centre of the pole figure appear to deform by 'easy slip' but keep their *c*-axis orientation constant owing to the specific operation of slip systems, whereas other grain orientations are continuously changed by the subgrain rotation recrystallisation.

5. Discussion and conclusions

The investigations presented above clearly show that the applied SEM electron diffraction techniques (OC imaging, ECP and EBS techniques) are a suitable set of tools to study the mechanisms and the influence of recrystallisation on texture development in naturally deformed quartz polycrystals. Furthermore, they are well suited to investigate the homogeneity as well as the development of textures and microstructures down to the grain and subgrain scale.

It was found that the microstructural and textural changes within the quartz fabric of both investigated sample series have been significantly influenced by dynamic recrystallisation. The microstructural observations, in conjunction with analyses of local orientation relationships on the subgrain level, allow criteria to be established which unambiguously characterise the dominant recrystallisation process.

In the case of dynamic recrystallisation by dominant GBM a characteristic statistical low between 5 and 15° in the frequency distribution of misorientation angles, i.e. at the transition from low- to high-angle grain boundaries, is clearly observed. This 'transition gap' as well as a similar relative frequency of subgrain boundary misorientations in the fine and coarse domains are indicative of a continuous formation and consumption of subgrain boundaries during *dynamic* grain growth. It appears that most subgrain boundaries are not able to develop misorientations $>5°$ at the generally high boundary mobility under low stresses and high deformation temperatures. The 'transition gap' may thus document a preferential removal of boundaries in the 5–15° range owing to the lower migration rate compared with the high-angle boundaries $>15°$, which is well known from studies on metals (e.g. Poirier, 1985). Hence, there is no formation of new grain boundaries but an extensive migration of existing boundaries.

In contrast, dynamic recrystallisation by subgrain rotation is characterised by a continuous transition from 0 to $>10°$ in the frequency distribution of misorientation angles, i.e. at the transition from low- to high-angle grain boundaries. The reason for this may be a high continuous build-up of dislocations under relatively high stresses and high deformation temperatures, leading to a progressive rotation of the subgrains. Towards higher misorientations of the subgrain boundaries, recrystallised grain boundaries are formed.

In both investigated sample suites a general texture strengthening with specific grain orientations being preferred during crystal plastic deformation and recrystallisation can be observed. It was found that the texture development during dynamic recrystallisation is evidently controlled by a differential activation of slip systems in grains of 'soft' and 'hard' orientations.

The 'soft' orientations (the Max. I and II texture components in the metaquartzites and the orientations with a central *c*-axis maximum in the quartz-ribbon mylonites) show the following characteristic features:

- well-defined misorientation axis clusters and simple axial dispersion paths which are indicative of 'easy slip' on a dominant slip system;
- a preferred alignment of subgrain boundary traces perpendicular to the dominant slip direction;
- a low density of widely spaced, straight subgrain boundaries and a higher ECP or EBSP pattern quality indicative of lower internal strain energies.

The 'hard' orientations (orientations deviating from the dominant texture components and pole figure maximum), in contrast, show:

- complex misorientation axis distributions or axial dispersion paths which indicate various interacting slip systems;
- no or less preferred alignment of subgrain boundary traces;
- a complex subgrain microstructure and lower ECP or EBSP pattern quality indicative of higher internal strain energies.

As a result the 'soft' grain orientations 'succeed' during subgrain rotation and/or grow preferentially during grain growth by GBM at the expense of the 'hard' grain orientations. Hence, these results give consistent answers to the question of whether 'soft' or 'hard' grain orientations are preferred during crystal plastic deformation and recrystallisation, which has been controversially discussed in the literature (cf. Urai et al., 1986; Knipe and Law, 1987; Karato, 1988; Gleason et al., 1993). Furthermore, they show the significance of qualitatively identifying relative internal strain energies of specific grain orientations by means of: (1) the quality of the analysed ECP or EBSP (a qualitative measure of relative dislocation densities); (2) the relative density of subgrain boundaries; (3) the relative abundance of subgrain misorientations.

For the determination of specific crystal slip systems which are responsible for the observed axial dispersion patterns and subgrain misorientation distributions, the interpretative model in Fig. 2 was used. The model is strictly confined to polygonised subgrain microstructures with straight boundaries indicative of a dominant proportion of tilt boundaries.

Apart from the determination of slip systems, the detailed analysis of distribution and degree of preferred subgrain misorientations provides evidence for those crystallographic orientations which are preferred for 'easy slip' and which are therefore not able to build up high internal strain energies. These data, as well as an unambiguous distinction of the recrystallisation processes, are of vital importance for a quantitative modelling of texture development during recrystallisation (Jessell and Lister, 1990; Wenk et al., 1997). Similar data could be incorporated into future research and may contribute to a better understanding of the texture development in recrystallised quartz polycrystals.

Beside intracrystalline slip and recrystallisation, the influence of twinning after the Dauphiné law was also investigated. The Dauphiné twins observed within the samples are complex interpenetration twins and presumably generated as growth twins during the phase transition between high and low quartz (cf. Frondel, 1962; Barber and Wenk, 1991). It was shown that the population of Dauphiné twins is gradually reduced with progressive deformation (quartz-ribbon mylonites) or grain growth (metaquartzites). This, together with observations of migrating twin boundaries as well as of a penetrative deformation in both hosts and twins, clearly indicated a generation of twins prior to the deformation. There are no indications for a generation of preferred orientation for slip due to the twin operation, so that a mechanical origin for the twins (cf. Tullis and Tullis, 1972) and a possible influence on texture development can clearly be discarded.

The frequency and spatial distribution of high-angle misorientations does not provide any evidence for a preferred mobility or stability of specific grain boundaries during dynamic recrystallisation. Further input on the significance of preferred high-angle misorientations may come from future analyses applying the coincident site lattice model (cf. McLaren, 1986).

Acknowledgements

This work was presented at the 'International Conference on Textures and Physical Properties of Rocks', Göttingen, October 1999. I would like to thank Klaus Weber and Werner Skrotzki for the support during the project, as well as the DAAD, the DFG and the Land Niedersachsen for providing the financial support. Geoff Lloyd is thanked for introducing me to the electron diffraction techniques and hosting me at various times at Leeds University. The help from and discussions with Martin Casey, Martyn Drury, Andy Farmer, Florian Heidelbach, Karsten Kunze, Bernd Leiss, Dave Mainprice, Dave Prior, Klaus Ullemeyer, Niels Schmidt and Pat Trimby during the past years are greatly acknowledged. The constructive reviews of Florian Heidelbach and Pat Trimby were very welcome. Last but not least I would like to thank Bernd Leiss and Klaus Ullemeyer for organising this sociable and stimulating meeting.

References

Adams, B.L., Wright, S.I., Kunze, K., 1993. Orientation imaging: the emergence of a new microscopy. Metallurgical and Materials Transactions 24A, 819.

Barber, D.J., Wenk, H.-R., 1991. Dauphiné twinning in deformed quartzites: implications of an in situ TEM study of α–β phase transformation. Physics and Chemistry of Minerals 17, 492–502.

Dingley, D.J., 1984. Diffraction from sub-micron areas using electron backscattering in a scanning electron microscope. Scanning Electron Microscopy II, 569–575.

Dingley, D.J., Randle, V., 1992. Microtexture determination by electron backscatter diffraction. Journal of Material Science 27 (17), 4545–4566.

Dornbusch, H.J., 1995. Gefüge-, Mikrostruktur- und Texturuntersuchungen an Hochtemperatur-Scherzonen in granulitfaziellen Metabasiten der Ivrea-Zone. Geotektonische Forschungen 83 94 pp.

Drury, M.R., Urai, J.L., 1990. Deformation-related recrystallization processes. Tectonophysics 172, 235–253.

Engler, O., Gottstein, G., Pospiech, J., Jura, J., 1994. Statistics, evaluation and representation of single grain orientation measurements. In: Bunge, H.J. (Ed.), Proceedings of the 10th International Conference on Textures of Materials, Materials Science Forum 157–162, pp. 259–274.

Etchecopar, A., 1977. A plane kinematic model of progressive deformation in a polycrystalline aggregate. Tectonophysics 39, 121–139.

Farmer, A.B., 1992. A microstructural investigation of natural deformation in quartz aggregates. Ph.D. thesis, University of Leeds, 307 pp.

Frondel, C., 1962. Dana's System of Mineralogy. Wiley, New York, 334 pp.

Gleason, G.C., Tullis, J, Heidelbach, F., 1993. The role of dynamic recrystallization in the development of lattice preferred orientations in experimentally deformed quartz aggregates. Journal of Structural Geology 15, 1145–1168.

Green, H.W., Griggs, D.T., Christie, J.M., 1970. Syntectonic and annealing recrystallisation of fine-grained quartz aggregates. In: Paulitsch, P. (Ed.), Experimental and Natural Rock Deformation. Springer-Verlag, Berlin, pp. 272–335.

Heidelbach, F., 1994. Textures and microstructures in recrystallized rocks; a study by X-ray and electron diffraction. Ph.D. thesis, University of California at Berkeley, 165 pp.

Heidelbach, F., Kunze, K., Wenk, H.-R., 2000. Texture analysis of a recrystallized quartzite using electron diffraction in the scanning electron microscope. Journal of Structural Geology 22, 91–104.

Hobbs, B.E., 1985. The geological significance of microfabric analysis. In: Wenk, H.R. (Ed.), Preferred Orientations in Deformed Metals and Rocks. Academic Press, London, pp. 463–484.

Humphreys, F.J., 1988. Experimental techniques for microtexture determination. In: Kallend, J.S., Gottstein, G. (Eds.), Eighth International Conference on Textures of Materials (ICOTOM 8), The Metallurgical Society, pp. 171–182.

Humphreys, F.J., 1999. Quantitative metallography by electron backscattered diffraction. Journal of Microscopy 195, 170–185.

Jacobs, J., Thomas, R.J., Weber, K., 1993. Accretion and indentation tectonics at the southern edge of the Kaapvaal craton during the Kibaran (Grenville) orogeny. Geology 21, 203–206.

Jessell, M.W., 1987. Grain-boundary migration microstructures in a naturally deformed quartzite. Journal of Structural Geology 9, 1007–1014.

Jessell, M.W., 1988a. Simulation of fabric development in recrystallizing aggregates—I. Description of the model. Journal of Structural Geology 10, 771–778.

Jessell, M.W., 1988b. Simulation of fabric development in recrystallizing aggregates—II. Example model runs. Journal of Structural Geology 10, 779–793.

Jessell, M.W., Lister, G.S., 1990. A simulation of the temperature dependence of quartz fabrics. In: Knipe, R.J., Rutter, E.H. (Eds.), Deformation Mechanisms, Rheology and Tectonics. Geological Society, pp. 353–362 Special Publications 54.

Karato, S.-I., 1988. The role of recrystalization in the preferred orientation of olivine. Physics of the Earth and Planetary Interiors 51, 107–122.

Knipe, R.J., Law, R.D., 1987. The influence of crystallographic orientation and grain boundary migration on microstructural and textural evolution in an *S-C* mylonite. Tectonophysics 135, 155–169.

Kunze, K., Adams, B.L., Heidelbach, F., Wenk, H.-R., 1994. Local microstructural investigations in recrystallized quartzite using orientation imaging microscopy. In: Bunge, H.J. (Ed.), Proceedings of the 10th International Conference on Textures of Materials, Materials Science Forum 157–162, pp. 1243–1249.

Law, R.D., 1990. Crystallographic fabrics: a selective review of their application to research in structural geology. In: Knipe, R.J., Rutter, E.H. (Eds.), Deformation Mechanisms, Rheology and Tectonics. Geological Society, pp. 335–352 Special Publications 54.

Leiss, B., Barber, D.J., 1999. Mechanisms of dynamic recrystallization in naturally deformed dolomite inferred from EBSP analyses. Tectonophysics 303, 51–69.

Lister, G.S., Paterson, M.S., Hobbs, B.E., 1978. The simulation of fabric development and its application to quartzite: the model. Tectonophysics 45, 107–158.

Lloyd, G.E., 1987. Atomic number and crystallographic contrast images with the SEM: a review of backscattered electron techniques. Mineralogical Magazine 51, 3–19.

Lloyd, G.E., 1994. An appreciation of the SEM electron channelling technique for petrofabric and microstructural analysis of geological materials. In: Bunge, H.J., Siegesmund, S., Skrotzki, W., Weber, K. (Eds.), Textures of Geological Materials, DGM Informationsgesellschaft, Oberursel, pp. 109–126.

Lloyd, G.E., Freeman, B., 1994. Dynamic recrystallisation of quartz under greenschist conditions. Journal of Structural Geology 16, 867–881.

Lloyd, G.E., Farmer, A.B., Mainprice, D., 1997. Misorientation analysis and the formation and orientation of subgrain and grain boundaries. Tectonophysics 279, 55–78.

McLaren, A.C., 1986. Some speculations on the nature of high-angle grain boundaries in quartz rocks. In: Hobbs, B.E., Heard, H.C. (Eds.), Mineral and Rock Deformation, Laboratory Studies—The Paterson Volume, American Geophysical Union, pp. 233–246 Monograph 36.

Neumann, B., 1996. Texturbildende Prozesse in rekristallisierten Quarzpolykristallen -Einzelkorn-und Gesamttexturanalysen. Geotektonische Forschungen 87 154 pp..

Olesen, N.Ø., Schmidt, N.-H., 1990. The SEM/ECP technique applied on twinned quartz crystals. In: Knipe, R.J., Rutter, E.H. (Eds.), Deformation Mechanisms, Rheology and Tectonics. Geological Society, pp. 369–373 Special Publications 54.

Pospiech, J., Lücke, K., Sztwiertnia, K., 1993. Orientation distribution and orientation correlation functions for the description of microstructures. Acta Metallurgica et Materialica 41, 305–321.

Prior, D.J., 1999. Problems in determining the misorientation axes, for small angular misorientations, using electron backscatter diffraction in the SEM. Journal of Microscopy 195, 217–225.

Prior, D.J, Trimby, P.W., Weber, U.D., Dingley, D.J., 1996. Orientation contrast imaging of microstructures in rocks using forescatter detectors in the scanning electron microscope. Mineralogical Magazine 60, 859–869.

Randle, V., 1992. Microtexture Determination and its Applications. The Institute of Metals, London, 182 pp.

Rutter, E.H., Brodie, K.H., Evans, P.J., 1993. Structural geometry, lower crustal magmatic underplating and lithospheric strechting in the Ivrea-Verbano zone, northern Italy. Journal of Structural Geology 15, 647–662.

Sander, B., 1950. Einführung in die Gefügekunde der geologischen Körper. Band 2, Springer Verlag, Vienna.

Schmid, S.M., Casey, M., 1986. Complete fabric analysis of some commonly observed quartz *c*-axis patterns. In: Hobbs, B.E., Heard, H.C. (Eds.), Mineral and Rock Deformation, Laboratory Studies—The Paterson Volume, American Geophysical Union, pp. 263–286 Monograph 36.

Schmid, S.M., Zingg, A., Handy, M., 1987. The kinematics of movements along the the Insubric Line and the emplacement of the Ivrea Zone. Tectonophysics 135, 47–66.

Schmidt, N.-H., Olesen, N.Ø., 1989. Computer-aided determination of crystal-lattice orientation from electron-channeling patterns in the SEM. Canadian Mineralogist 27, 15–22.

Trimby, P.W., Prior, D.J., Wheeler, J., 1998. Grain boundary hierarchy development in a quartz mylonite. Journal of Structural Geology 20, 917–935.

Tullis, J., Tullis, T., 1972. Preferred orientation of quartz produced by mechanical Dauphiné twinning: thermodynamics and axial experiments. In: Heard, H.C., Borg, I.Y., Carter, N.C., Raleigh, C.B. (Eds.), Flow and Fracture of Rocks, American Geophysical Union, pp. 67–82 Monograph 16.

Tullis, J., Christie, J.M., Griggs, D.T., 1973. Microstructure and preferred orientations of experimentally deformed quartzites. Bulletin of the Geological Society of America 84, 297–314.

Urai, J.L., Means, W.D., Lister, G.S., 1986. Dynamic recrystallisation of minerals. In: Hobbs, B.E., Heard, H.C. (Eds.), Mineral and Rock Deformation, Laboratory Studies—The Paterson Volume, American Geophysical Union, pp. 161–199 Monograph 36.

Wenk, H.-R., Christie, J.M., 1991. Comments on the interpretation of deformation textures in rocks. Journal of Structural Geology 13, 1091–1110.

Wenk, H.-R., Canova, G., Bréchet, Y., Flandin, L., 1997. A deformation based model for recrystallization of anisotropic materials. Acta Materialia 45, 3283–3296.

Wenk, H.-R., Matthies, S., Donovan, J., Chateigner, D., 1998. BEARTEX, a Windows-based program system for quantitative texture analysis. Journal of Applied Crystallography 31, 262–269.